


Generalized phenomenological model for the magnetic field penetration and magnetization hysteresis loops of a type-II superconductor

Wei Xie , Yu-Hao Liu , and Hai-Hu Wen *

National Laboratory of Solid State Microstructures and Department of Physics,
Collaborative Innovation Center of Advanced Microstructures, Nanjing University, Nanjing 210093, China

 (Received 20 August 2021; revised 7 December 2021; accepted 23 December 2021; published 5 January 2022)

A generalized phenomenological model for the mixed state of type-II superconductors with magnetic field parallel to the superconducting plate is proposed. This model considers the global magnetization including both the equilibrium magnetization from surface screening current and the nonequilibrium magnetization from bulk pinning in a self-consistent way. Our model can be used to simulate the magnetization hysteresis loops (MHLs) and flux penetrating process of different type-II superconductors, from low- to high- κ values. Here we take a $\text{Ba}_{0.6}\text{K}_{0.4}\text{Fe}_2\text{As}_2$ single crystal and pure Nb plate as testing examples. The model can fit the data quite well and several important parameters can be extracted from the fitting. Thus the model can be extended to a general case for studying the magnetization and flux penetration in other type-II superconductors.

DOI: [10.1103/PhysRevB.105.014505](https://doi.org/10.1103/PhysRevB.105.014505)

I. INTRODUCTION

Due to different signs of the interface energy between superconducting and normal regions [1], superconductors can be divided into two types: type-I superconductors with positive interface energy; type-II superconductors with negative interface energy. This categorization can be made based on the value of the Ginzburg-Landau (GL) parameter $\kappa = \lambda/\xi$, for type-I superconductors, $\kappa < 1/\sqrt{2}$ and for type-II superconductors, $\kappa > 1/\sqrt{2}$. For a clean type-I superconductor, there is a well-defined thermodynamic critical field H_c which can be measured directly. When the applied field is below H_c , the superconductor is in Meissner state. With the existence of surface screening supercurrent, flux can be fully expelled from the interior of superconductor. Above H_c , the superconductor will lose its superconductivity and go into normal state. For a clean type-II superconductor, there are two different critical fields, namely the lower critical field H_{c1} and the upper critical field H_{c2} . When the applied field is below H_{c1} , the superconductor is in Meissner state, just as the type-I superconductor. From H_{c1} to H_{c2} , the superconductor is in mixed state with vortices penetrating into the bulk region. Above H_{c2} , the superconductor is in normal state [1,2]. The determination of critical fields is important in the application of superconductors, such as the radio frequency superconducting cavities for the studies of high energy physics [3,4]. While in practice, there are defects, disorders and impurities in the superconductors, which can act as pinning centers of vortices [5–7]. In this case, in addition to the surface screening supercurrent, there exists a bulk supercurrent due to these pinning centers. This critical current induced by pinning plays an important role in the application of superconductors [8–11], and these superconductors with pinning centers are called dirty

type-II superconductors. In the magnetization hysteresis loops (MHLs) of these type-II superconductors, hysteresis can be easily observed.

In order to calculate the magnetization of type-II superconductors, Bean *et al.* firstly proposed the critical state model [12–14] which can describe the flux penetration and vortex pinning, by assuming that (1) the pinning force is uniform and independent of local magnetic field; (2) the Lorentz force is equal to the pinning force everywhere inside the superconductor. In the original model, the critical current density J_c calculated from magnetization is constant and independent of the applied field at a given temperature. This leads to a flat and parallel MHL both in the field ascending and descending processes. While in most experiments, it was found that the width of MHL curves will either decrease or increase with varying magnetic field [15–17]. To understand this phenomenon, Kim *et al.* assumed that the critical current density J_c due to bulk pinning is inversely proportional to the field, i.e., $J_c(H_i) = k/(A_1 + |H_i|)$ [18–21], where H_i is the local magnetic field. Afterwards, many other models were proposed for interpreting the field dependence of bulk pinning. For example, Watson *et al.* considered the J_c to be linearly proportional to the field $J_c(H_i) = A_2 + B_2|H_i|$ [22]; Irie *et al.* proposed a power-law relationship $J_c(H_i) = k/(|H_i|)^n$ [23,24]; Fitz *et al.* introduced an exponential-law relationship $J_c(H_i) = J_c(0) \exp(-|H_i|/A_3)$ [25–27]; Xu *et al.* adopted a general form of J_c given by $J_c(H_i) = J_c(0)/(1 + |H_i|/A_4)^n$ [28]. In above equations, A_1 , A_2 , B_2 , k , A_3 , and A_4 are fitting parameters.

Additionally, for the magnetization of low- κ type-II superconductors, Kes *et al.* suggested to divide the magnetization into reversible part and irreversible part [29]. Following this idea, Chen *et al.* also proposed an extended critical state model by combining the equilibrium magnetization and an energy barrier of the surface layer, together with the nonequilibrium magnetization of the bulk region, the latter is described by

*hhwen@nju.edu.cn

the critical state model with modified boundary conditions [30–35]. Furthermore, Gokhfeld *et al.* proposed a modified critical state model by assuming a field-dependent thickness of surface layer with screening current [36,37]. When the magnetic field is reduced from a positive high value to less than H_{c1} , there are still a lot of vortices inside the superconductor, while the surface screening layer looks like that in the initial Meissner state. We call this state as vortex-trapped Meissner state. This has never been seriously dealt in previous models, only Matsushita *et al.* had a rough and macroscopic investigation on it and put forward another modified critical state model [38]. Brandt *et al.* also considered the isotropy and anisotropy of superconductors with two different kinds of pinnings in their J_c dependence for the critical state model and did some calculations on the global magnetization [39].

However, none of these models mentioned above can describe the magnetization of most type-II superconductors with different κ values or ratios of H_{c2}/H_{c1} . We try to deal with this problem mathematically and take different kinds of type-II superconductors into consideration, and thus give a simple phenomenological model for the vortex critical state in this paper. To validate our model, we measured the MHLs of a $\text{Ba}_{0.6}\text{K}_{0.4}\text{Fe}_2\text{As}_2$ single crystal and a pure Nb plate and found that the model fits experimental data in a self-consistent way. This paper is organized as follows. Section II introduces the basic assumptions of our model. Sections III and IV give a brief description of the flux penetrating process and calculation of magnetization, respectively. Section V gives the results of experiments and numerical fittings. Section VI gives a conclusion of our paper.

II. BASIC ASSUMPTIONS OF THE MODEL

Our model divides the magnetization into two major contributions, namely the equilibrium magnetization and the nonequilibrium magnetization, as adopted by Kes *et al.* and Chen *et al.* [29–31,40]. A complete MHL curve involves eight different stages with the applied field H_a firstly increased from 0 to the maximum magnetic field H_m , then changed from H_m to $-H_m$, and lastly changed from $-H_m$ to H_m . In this section, we firstly handle with the equilibrium magnetization of type-II superconductors. Then, we deal with the nonequilibrium magnetization using a modified critical state model. Finally, we give a discussion on the vortex-trapped Meissner state both in the field descending and ascending process.

A. Equilibrium magnetization

For the equilibrium magnetization, we consider a clean type-II superconductor without pinning centers inside the sample. It has a reversible magnetization curve $M(H)$ with two thermodynamic critical fields, namely H_{c1} and H_{c2} . In order to calculate the magnetization, we separate the superconductor into two regions, the bulk region and a surface layer surrounding it [30]. The shielding current is flowing in the surface layer which is in the order of London penetration depth λ_L . When the applied field is less than the lower critical field, i.e., $H_a < H_{c1}$, the superconductor is in Meissner state. The shielding supercurrent is flowing in the surface layer, and thus there exists a boundary between the surface layer and

the inner bulk region. We define the field at the boundary $x = \lambda_L$ as H_e . In this case, the effective boundary field H_e should be zero, as well as the field in bulk region. When $H_{c1} < H_a < H_{c2}$, the superconductor is in the mixed state and the shielding effect of surface supercurrent will be gradually reduced. Flux lines start to penetrate into the bulk region at $H_a = H_{c1}$. As there are no pinning centers, and thus no bulk supercurrent inside the superconductor, the field in the bulk region should be uniform and equal to H_e . In the surface layer, the magnetic field decays exponentially in space from H_a to H_e , in the scale of London penetration depth λ_L [41]. When $H_a > H_{c2}$, the superconductor is in normal state and the field everywhere is equal to H_a . Following these discussions, when the superconductor is in mixed state, we propose a general relation between H_e and H_a :

$$M_{\text{equ}} = -\frac{H_{c1}(H_{c2} - H_a)}{H_{c2} - H_{c1}} \left(\frac{H_{c1}}{H_a}\right)^\alpha. \quad (1)$$

$$H_e = M_{\text{equ}} + H_a. \quad (2)$$

Here H_{c1} and H_{c2} are the lower critical field and the upper critical field, respectively. α is a dimensionless fitting parameter. M_{equ} is the equilibrium magnetization. This relation satisfies the boundary conditions of the mixed state: when $H_a = H_{c1}$, the mixed state has $M_{\text{equ}} = -H_{c1}$, $H_e = 0$; when $H_a = H_{c2}$, the mixed state has $M_{\text{equ}} = 0$, $H_e = H_{c2}$. The derivative of M_{equ} with respect to H_a is the magnetic susceptibility of the equilibrium magnetization curve which is defined as χ_{equ} :

$$\chi_{\text{equ}} = \frac{dM_{\text{equ}}}{dH_a} = \frac{H_{c1}}{H_{c2} - H_{c1}} \left(\frac{H_{c1}}{H_a}\right)^\alpha \left[1 + \frac{\alpha(H_{c2} - H_a)}{H_a}\right]. \quad (3)$$

When $H_a = H_{c2}$, we have

$$\chi_{\text{equ},c2} = \frac{H_{c1}}{H_{c2} - H_{c1}} \left(\frac{H_{c1}}{H_{c2}}\right)^\alpha. \quad (4)$$

In this way, the fitting parameter α can be written as

$$\alpha = \ln \left(\frac{(H_{c2} - H_{c1})\chi_{\text{equ},c2}}{H_{c1}} \right) / \ln \left(\frac{H_{c1}}{H_{c2}} \right). \quad (5)$$

If H_{c2} is much larger than H_{c1} ($H_{c1} \ll H_{c2}$, especially for high- κ superconductors, such as cuprate and iron-based superconductors), the equation can be simplified to

$$\alpha = -1 + \ln(\chi_{\text{equ},c2}) / \ln \left(\frac{H_{c1}}{H_{c2}} \right). \quad (6)$$

The H_{c2} is always tens or hundreds of Tesla and difficult to be achieved in experiment. Thus we may also pay some attention to the magnetic susceptibility at the lower critical field. When $H_a = H_{c1}$, we have

$$\chi_{\text{equ},c1} = \frac{H_{c1}}{H_{c2} - H_{c1}} + \alpha. \quad (7)$$

The fitting parameter α can be written as

$$\alpha = \chi_{\text{equ},c1} - \frac{H_{c1}}{H_{c2} - H_{c1}}. \quad (8)$$

If $H_{c1} \ll H_{c2}$, the fitting parameter α is right the magnitude of the magnetic susceptibility at H_{c1} . Above all, if we know three

of the four variables $\chi_{\text{equ},c1}$ or $\chi_{\text{equ},c2}$, H_{c1} , H_{c2} , α , the last one can be easily obtained.

As a comparison, the reversible relation of the mixed state adopted by Kes *et al.* fit experimental data only in the high temperature region for low- κ type-II superconductors [29]. Chen *et al.* used an exponential relation of H_e and H_a when the maximum magnetic field H_m is much lower than H_{c2} [30]. However, when H_a is close enough to H_{c2} or the κ is high, the relation $H_e(H_a)$ is inclined to be a straight line [42,43]. Our relation combines the merits of both ideas above. In the low field limit (H_a is close to H_{c1}), if $H_{c1} \ll H_{c2}$, the relation can be simplified to a power law:

$$M_{\text{equ}} \propto -H_a^{-\alpha}, \quad (9)$$

with $(H_{c2} - H_a)/(H_{c2} - H_{c1}) \rightarrow 1$. However, this case ($H_{c1} \ll H_{c2}$) was not considered in the model of Kes, in which the relation $B(H_a)$ was simplified to a linear one and is not consistent with the experiment [29]. In the high field limit (H_a is close to H_{c2}), if $H_{c1} \ll H_{c2}$, the M_{equ} in Eq. (1) is small compared with H_a and our relation $H_e(H_a)$ is approximately to be a straight line, which is consistent with that suggested by Campbell *et al.* [44].

For simplicity, we assume the spatial distribution of field in the surface layer to be linear. This can serve as a good approximation when the sample dimension is much larger than the London penetration depth λ_L . Furthermore, the London penetration depth λ_L is related to the measuring temperature and this will lead to a more complicated relation [36,37]. In our model, we assume λ_L to remain unchanged with magnetic field for simplicity. The fitting will be done for magnetization hysteresis loop measured at a particular temperature, thus the penetration depth λ_L is a parameter with a preset value for each temperature.

B. Nonequilibrium magnetization

For the nonequilibrium magnetization, it is a little different because of the existence of pinning centers. For a type-II superconductor with pinning centers, the magnetization hysteresis $M(H)$ is irreversible. Under our assumptions, the shielding effect of surface layer is just the same as the equilibrium part introduced above. The boundary field H_e is self-consistently determined by the same value at the boundary, which connects the surface screening layer and the bulk region, as Eqs. (1) and (2). While for the bulk region, the flux motion should be prevented due to the existence of pinning centers. Bean *et al.* [12,13] proposed a critical state, in which the pinning force and the magnetic pressure (or Lorenz force) originating from the gradient of magnetic field are in equilibrium. Thus the field in the bulk region will not be uniform anymore. In this case, the superconductor can carry a critical current which obeys the law $\nabla \times B = \mu_0 J_c$, with B the local average density of the magnetic induction. For simplicity, in the following calculations or equations, we neglect the μ_0 . In the critical state model, this pinning force is equal to Lorenz force $\Phi_0 J_c$ (Φ_0 is flux quantum). There are different forms of J_c with respect to magnetic field proposed previously, as we have discussed in section I. However, most of these models did not consider the upper critical field H_{c2} in their J_c equations. In fact, the critical current density J_c should be zero when the

applied field H_a approaches H_{c2} . To deal with this problem, we assume a more general form of J_c in our model, this gives not only a self-consistent formula of the boundary field H_e , but also on the lower critical field H_{c1} and the upper critical field H_{c2} , as shown by the following equation:

$$J_c = J_{c0} \frac{H_{c2} - |H_e|}{H_{c2}} \left(\frac{H_{c1}}{H_{c1} + |H_e|} \right)^\beta. \quad (10)$$

Here, β is a dimensionless fitting parameter. J_{c0} is the critical current density when the field is zero. This relation satisfies the experimental variation of critical current density very well. When $H_e = 0$, the critical current density is equal to J_{c0} . When $H_e = H_{c2}$, the superconductor is in normal state and the critical current density is zero. In the low field limit (H_a is close to H_{c1}), if $H_{c1} \ll H_{c2}$, the equation can be simplified to a power law:

$$J_c \propto (H_{c1} + |H_e|)^{-\beta} \quad (11)$$

with $(H_{c2} - |H_e|)/H_{c2} \rightarrow 1$. When $\beta = 1$, the equation is right the relation adopted by Kim [18]. In the high field limit (H_a is close to H_{c2}), the equation tends to be a straight line, which is consistent with the experiment [45]. Above all, our equation treats the magnetic induction and critical current density in a more reasonable way. With the Maxwell equation for the one-dimensional superconductor $-dH(x)/dx = J_c$ and proper boundary conditions, we can calculate the spatial distribution of magnetic induction inside the superconductor.

C. Vortex-trapped Meissner state

In the field descending process, when the applied field H_a is decreased below H_{c1} , the superconductor will try to re-enter the Meissner state. However, this Meissner state is different from the initial Meissner state, as the bulk pinning is different in these two cases. In the initial Meissner state, no vortices penetrate into the bulk region, and thus, there is no bulk pinning current inside the superconductor. However, in the Meissner state of the field descending process, vortices will be trapped inside the superconductor and the bulk pinning current is not zero anymore. This vortex-trapped Meissner state will maintain when the field is ascending in the negative side with $H_a < -H_{c1}$. The remaining bulk pinning current is also different from the pinning current J_c given by Eq. (10) as $H_e = 0$, and we defined it as J_{cr} . From the experimental perspective, we can see a sudden change of the slope of the linear part from magnetization curve when $H_a < H_{c1}$ in these two cases. This is particularly obvious when the Ginzburg-Landau parameter κ is small or H_{c1} is in the same order of magnitude with H_{c2} [38]. This sudden change was not explained in the models of Chen [30] and Walmsley [46]. In their models, they assumed the bulk pinning in the superconductor to remain unchanged when $H_a < H_{c1}$ in the field descending process, which is clearly unreasonable. Because the flux distribution profile in the bulk region during this period varies remarkably, the magnetization arising from the bulk pinning will change along with the varying applied field. Matsushita *et al.* [38] dealt this problem and offered a phenomenological model with a perfect Meissner state layer and a flux trapped interior

part, and the boundary of both regions will move towards the interior region of the bulk with descending field.

Unlike these models mentioned above, we propose a new model to deal with this sophisticated situation, based on the ideas of critical state. In the field descending process, when the applied field H_a is decreased below H_{c1} , we assume the shielding supercurrent to be the same as the initial Meissner state. Thus the surface layer will be in full shielding state and the boundary field H_e is zero as before. For a vortex existing near the boundary of bulk region and surface layer, it feels Lorenz forces both from the shielding supercurrent J_s and the remaining bulk pinning current J_{cr} with opposite directions. These two forces, as well as the pinning force F_p from disorders and defects, form an equilibrium state $\Phi_0 J_s - \Phi_0 J_{cr} + F_p = 0$. When H_a is further decreased, the shielding supercurrent J_s , which is the gradient of magnetic field in the surface layer, will decrease simultaneously as a linear approximation $J_s \propto (H_a - H_e)/\lambda_L = H_a/\lambda_L$. Since J_s is related to the force preventing the trapped vortices from out-going, the remaining bulk pinning current J_{cr} in the bulk region will reduce in the same pace with the applied field H_a to form a new equilibrium state. Above all, we assume that J_{cr} varies linearly with H_a

$$J_{cr} = J_{c0} \frac{H_a - H_0}{H_{c1} - H_0}. \quad (12)$$

J_{c0} is the zero-field critical current density from equation Eq. (10), H_{c1} is the lower critical field, H_0 is the field at which the remaining pinning current density reduces to zero. When $H_a = H_{c1}$, $J_{cr} = J_{c0}$, and when $H_a = H_0$, $J_{cr} = 0$. In this case, the magnetization of the vortex-trapped Meissner state in our model is linearly varying with applied field, as well as the initial Meissner state. In the next section, we will prove in detail that, H_0 can be simply obtained from fitting to the experimental data, which is the intersection point of extended lines of magnetization curves from both the initial Meissner state and the vortex-trapped Meissner state.

The description of magnetization in other stages, for example from $H_a = -H_{c1}$ to $-H_m$ (with $H_m \gg H_{c1}$) and from $-H_m$ to zero will be the replica of the status mentioned above.

III. SPATIAL DISTRIBUTION OF MAGNETIC INDUCTION IN DIFFERENT REGIONS

After establishing the model as mentioned in section II, the magnetization in different stages of applying magnetic field can be obtained. The superconductor in our model is assumed to be a plate with infinite lateral sizes and thickness of $2d$ along x axis, which is illustrated in Fig. 1(a). The magnetic field H_a is applied parallel to the plate and enters from both sides of it. For convenience, we set the field direction along z axis, and as a consequence, the demagnetization factor is close to zero [47]. Due to the symmetry of the plate, the distribution of field or current is one-dimensional along x axis. Thus we take the cross-section of this plate along x -axis, as illustrated in Fig. 1(b). In Fig. 1(b), $x = 0$ represents the interface of superconductor and vacuum, λ_L is the London penetration depth which is much smaller than the sample dimension ($\lambda_L \ll 2d$), $x = d$ is the center of the plate. We

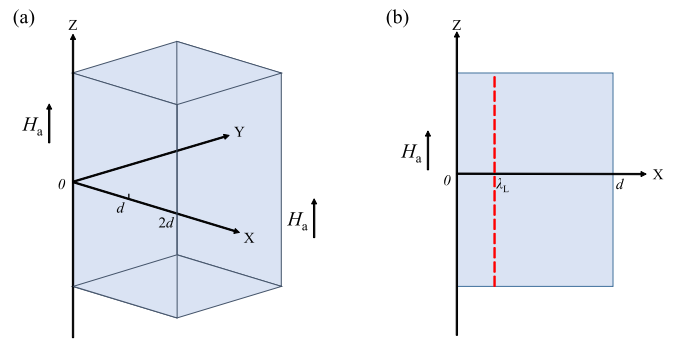


FIG. 1. Sketch of an infinite large superconducting plate. (a) The superconducting plate with thickness of $2d$ along x axis. The field is applied along z axis. (b) The cross-section of half plate in (a) along x axis. The light blue region indicates the superconducting plate. The red dashed line shows the boundary of surface layer and bulk region. The London penetration depth λ_L is much smaller than the thickness of the plate $2d$ ($\lambda_L \ll 2d$). Here we have magnified λ_L to make the surface layer discernible.

have only shown half of the plate in Fig. 1(b) and another half can be obtained directly with mirror symmetry of $x = d$.

A global MHL can be divided into eight different stages which will be discussed in detail below. Before magnetization measurement, the superconductor should be zero-field cooled down to a certain temperature, which is below the critical temperature T_c . The field distribution in the surface layer is $H_s(x)$ (with $0 < x < \lambda_L$) and in the bulk region is $H_b(x)$ (with $\lambda_L < x < d$). For simplicity, the field distributions of both surface layer and bulk region are linear in space. If $H_{c1} < H_m < H_{c2}$, details of the eight stages are as follows:

Stage (i). The initial Meissner state with H_a increased from 0 to H_{c1} . The magnetic field is confined in the surface layer which is in the order of λ_L , and H_e is zero. Vortices are not formed yet and no vortex penetration occurs in the bulk region. Thus there is only the equilibrium magnetization. For this stage, we have the field distribution as follows (as shown in Fig. 2)

$$H_s(x) = \frac{H_a}{\lambda_L}(\lambda_L - x), \quad (13)$$

$$H_b(x) = 0. \quad (14)$$

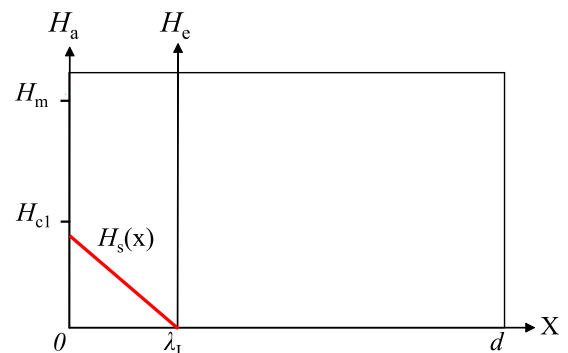


FIG. 2. Magnetic field distribution (red line) of a superconductor in stage (i) (the initial Meissner state with $H_a < H_{c1}$). $H_s(x)$ is the distribution function in the surface layer.

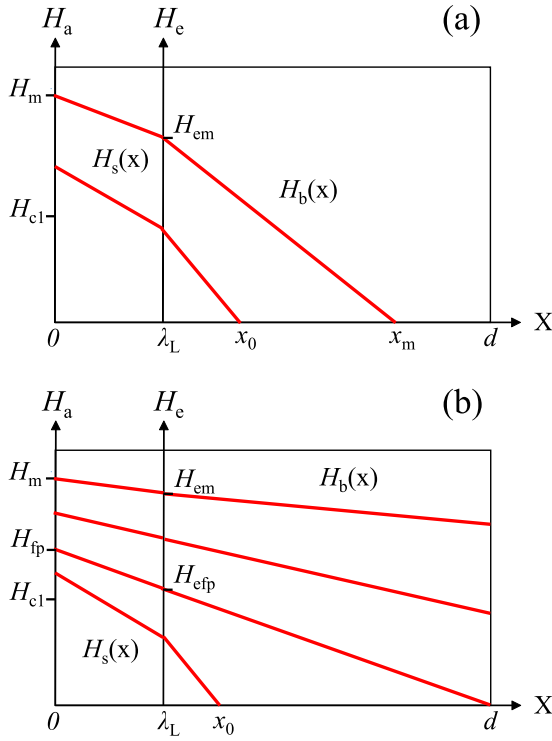


FIG. 3. Magnetic field distribution (red lines) of a superconductor in stage (ii) (the initial penetration process with $H_{c1} < H_a < H_m$) if (a) $H_m < H_{fp}$ and (b) $H_m > H_{fp}$. $H_s(x)$ is the distribution function in the surface layer. $H_b(x)$ is the distribution function in the bulk region.

Stage (ii). The initial penetration process with H_a increased from H_{c1} to $H_m (< H_{c2})$. The superconductor is in mixed state and the shielding effect of surface layer will be partially reduced. And thus, vortices start to penetrate into the bulk region. There are both equilibrium magnetization and nonequilibrium magnetization. We define the field where the sample is fully penetrated by the vortices as H_{fp} . There are two cases in this stage: $H_m < H_{fp}$ and $H_m > H_{fp}$. In the former case, we have the field distribution as follows [as shown in Fig. 3(a)]

$$H_s(x) = -\frac{x}{\lambda_L}(H_a - H_e) + H_a. \quad (15)$$

$$H_b(x) = \begin{cases} -J_c(x - \lambda_L) + H_e & \lambda_L < x < x_0 \\ 0 & x_0 < x < d \end{cases}. \quad (16)$$

In the above equations, H_e is the boundary field between the surface layer and the bulk region, which is connected with the applied field H_a by Eqs. (1) and (2). J_c is the bulk pinning current density, which is connected with H_e by Eq. (10). x_0 is the frontier of the vortices, which is

$$x_0 = \frac{H_e}{J_c} + \lambda_L. \quad (17)$$

The fully penetration field H_{fp} can be obtained in the following way. When $H_a = H_{fp}$, the boundary field is $H_{efp} = H_e[H_{fp}]$ and the flux front reaches right at the center of the superconductor $x_0 = d$. Thus we have

$$H_{efp} = J_c(d - \lambda_L). \quad (18)$$

We calculate Eqs. (18) and (10) to get H_{efp} , and the fully penetration field H_{fp} can therefore be obtained from Eqs. (1) and (2).

If $H_m > H_{fp}$, the situation is somewhat complicated. When $H_a < H_{fp}$ (or the flux front position x_0 is less than the sample thickness $x_0 < d$), the field distribution functions are just described by Eqs. (15) and (16). When $H_a > H_{fp}$ (or $x_0 > d$), the superconductor has been fully penetrated by vortices. The field distribution $H_s(x)$ is described by Eq. (15) and the $H_b(x)$ is given by [as shown in Fig. 3(b)]

$$H_b(x) = -J_c(x - \lambda_L) + H_e. \quad (19)$$

Stage (iii). The field descending process in the positive side with H_a decreased from H_m to H_{c1} . The superconductor is still in mixed state. The bulk pinning current will change its direction from the outer part of bulk region, while the inner part remains unchanged. We define the position where the bulk pinning current changes its direction as x_1 . The field distribution is continuous at this crossing point. This stage can also be divided into two cases: $H_m < H_{fp}$ and $H_m > H_{fp}$. When $H_a = H_m$, $H_e = H_{em}$ and $J_c = J_{cm}$. If $H_m < H_{fp}$, the flux will not fully penetrate the superconductor and the maximum penetration depth is defined as x_m

$$x_m = \frac{H_{em}}{J_{cm}} + \lambda_L. \quad (20)$$

The position x_1 can be obtained by

$$x_1 = \frac{H_{em} - H_e}{J_{cm} + J_c} + \lambda_L. \quad (21)$$

In this way, $H_s(x)$ is described by Eq. (15) and $H_b(x)$ is as follows [as shown in Fig. 4(a)]

$$H_b(x) = \begin{cases} J_c(x - \lambda_L) + H_e & \lambda_L < x < x_1 \\ -J_{cm}(x - \lambda_L) + H_{em} & x_1 < x < x_m \\ 0 & x_m < x < d \end{cases}. \quad (22)$$

If $H_m > H_{fp}$, the position where the critical current changes its direction x_1 is also obtained by Eq. (21). With decreasing the applied field, the opposite direction current will gradually penetrate the superconductor and the dividing line $x = x_1$ is approaching the center of superconductor $x = d$. In this case, the field distribution $H_s(x)$ is described by Eq. (15). When $x_1 < d$, $H_b(x)$ is [as shown in Fig. 4(b)]

$$H_b(x) = \begin{cases} J_c(x - \lambda_L) + H_e & \lambda_L < x < x_1 \\ -J_{cm}(x - \lambda_L) + H_{em} & x_1 < x < d \end{cases}. \quad (23)$$

However when $x_1 > d$, $H_b(x)$ is given by [as shown in Fig. 4(b)]

$$H_b(x) = J_c(x - \lambda_L) + H_e. \quad (24)$$

Stage (iv). The vortex-trapped Meissner state with H_a firstly decreased from H_{c1} to 0 and then increased from 0 to $-H_{c1}$ in the negative side. The superconductor re-enters Meissner state, which is different from the initial Meissner state. Vortices are trapped in the bulk region, and thus, the nonequilibrium magnetization is not zero as stage (i). When H_a is decreased, the trapped vortices will go outwards and the remaining bulk pinning current density J_{cr} will change in the meantime, as described by Eq. (12). We also divide this stage

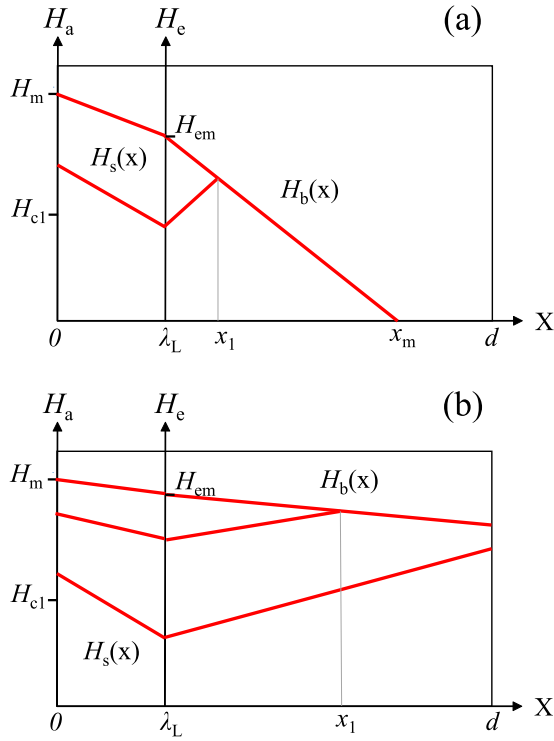


FIG. 4. Magnetic field distribution (red lines) of a superconductor in stage (iii) (the field descending process in the positive side with $H_{c1} < H_a < H_m$) if (a) $H_m < H_{fp}$ and (b) $H_m > H_{fp}$. $H_s(x)$ is the distribution function in the surface layer. $H_b(x)$ is the distribution function in the bulk region.

into two cases: $H_m < H_{fp}$ and $H_m > H_{fp}$. When $H_a = H_{c1}$, the initial dividing line x_1 [given by Eq. (21)] is defined as x_2 . If $H_m < H_{fp}$, there are critical currents with different directions in the bulk region and the new dividing line x_1 is given by

$$x_1 = \frac{H_{em}}{J_{cm} + J_{cr}} + \lambda_L. \quad (25)$$

The field distribution in the superconductor is [as shown in Fig. 5(a)]

$$H_s(x) = \frac{H_a}{\lambda_L}(\lambda_L - x). \quad (26)$$

$$H_b(x) = \begin{cases} J_{cr}(x - \lambda_L) & \lambda_L < x < x_1 \\ -J_{cm}(x - \lambda_L) + H_{em} & x_1 < x < x_m \\ 0 & x_m < x < d \end{cases}. \quad (27)$$

If $H_m > H_{fp}$ and $x_2 < d$, there are critical currents with different directions in the bulk region and the new dividing line x_1 is also given by Eq. (25). $H_s(x)$ is described by Eq. (26). $H_b(x)$ is [as shown in Fig. 5(b)]

$$H_b(x) = \begin{cases} J_{cr}(x - \lambda_L) & \lambda_L < x < x_1 \\ -J_{cm}(x - \lambda_L) + H_{em} & x_1 < x < d \end{cases}. \quad (28)$$

If $H_m > H_{fp}$ and $x_2 > d$, the critical current has only one direction in the bulk region. $H_s(x)$ is described by Eq. (26). $H_b(x)$ is [as shown in Fig. 5(c)]

$$H_b(x) = J_{cr}(x - \lambda_L) \quad (29)$$

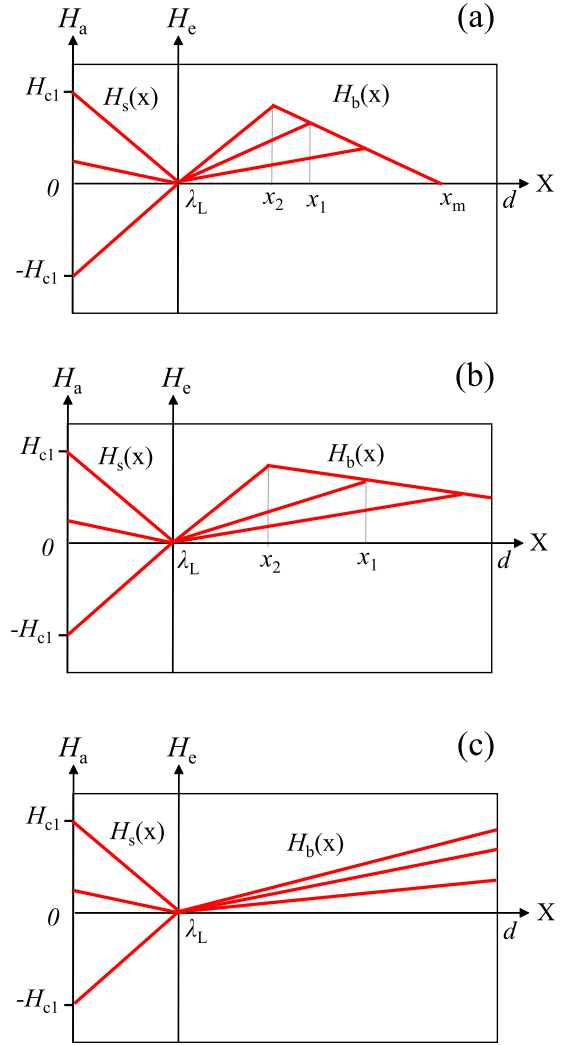


FIG. 5. Magnetic field distribution (red lines) of a superconductor in stage (iv) (the vortex-trapped Meissner state with $-H_{c1} < H_a < H_{c1}$) if (a) $H_m < H_{fp}$, (b) $H_m > H_{fp}$ and $x_2 < d$, and (c) $H_m > H_{fp}$ and $x_2 > d$. $H_s(x)$ is the distribution function in the surface layer. $H_b(x)$ is the distribution function in the bulk region.

The situations shown in Figs. 5(b) and 5(c) are two cases corresponding to strong and weak bulk pinning, respectively. During the calculation it depends on whether $x_2 < d$ or $x_2 > d$, the calculation program will directly determine that.

Stage (v). The field ascending process in the negative side with H_a increased from $-H_{c1}$ to $-H_m$. The superconductor is in mixed state and vortices with opposite direction start to penetrate the bulk region. The frontier of vortices with opposite direction is defined as x_0 and will move towards the center of superconductor. There should be annihilation of vortices with opposite vorticities at this moving frontier line. H_e is not zero but described by Eq. (1) and Eq. (2). The bulk pinning current density J_c of the penetrating part is given by Eq. (10). When $H_a = -H_{c1}$, $J_{cr} = J_{cr1}$. As in Stage (iv), if $H_m < H_{fp}$, the position x_0 is given by

$$x_0 = -\frac{H_e}{J_c} + \lambda_L. \quad (30)$$

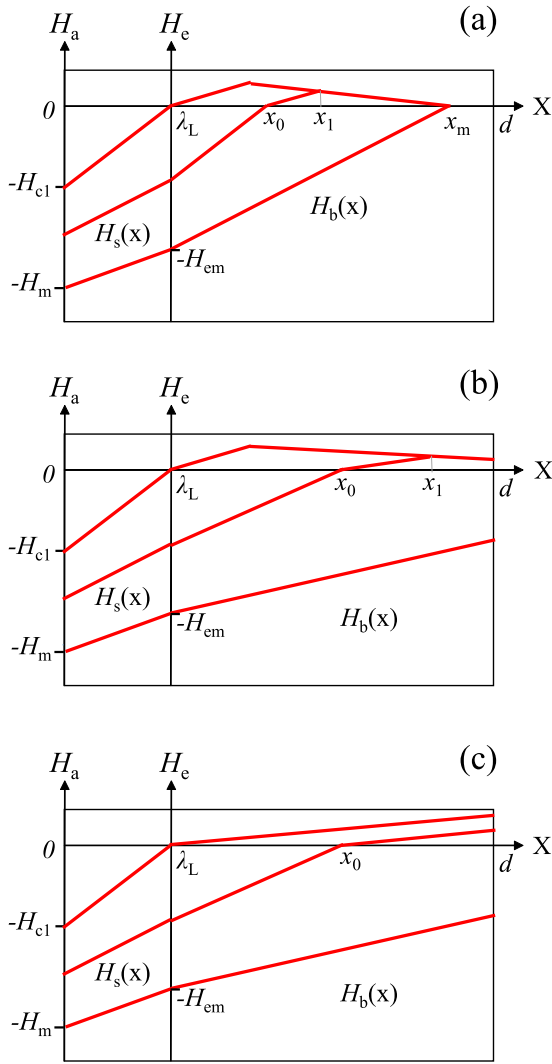


FIG. 6. Magnetic field distribution (red lines) of a superconductor in stage (v) (the field ascending process in the negative side with $-H_m < H_a < -H_{c1}$) if (a) $H_m < H_{fp}$, (b) $H_m > H_{fp}$ and $x_2 < d$, and (c) $H_m > H_{fp}$ and $x_2 > d$. $H_s(x)$ is the distribution function in the surface layer. $H_b(x)$ is the distribution function in the bulk region.

The position dividing currents with different directions x_1 is

$$x_1 = \frac{H_{em} + J_{cm}\lambda_L + J_{cr1}x_0}{J_{cm} + J_{cr1}}. \quad (31)$$

Thus the field distribution can be written as [see Fig. 6(a)]

$$H_s(x) = -\frac{x}{\lambda_L}(H_a - H_e) + H_a, \quad (32)$$

$$H_b(x) = \begin{cases} J_c(x - \lambda_L) + H_e & \lambda_L < x < x_0 \\ J_{cr1}(x - x_0) & x_0 < x < x_1 \\ -J_{cm}(x - \lambda_L) + H_{em} & x_1 < x < x_m \\ 0 & x_m < x < d \end{cases}. \quad (33)$$

If $H_m > H_{fp}$ and $x_2 < d$, there are remaining pinning currents with different directions in the bulk region. $H_s(x)$ is described

by Eq. (32). When $H_a < H_{fp}$, $H_b(x)$ is [as shown in Fig. 6(b)]

$$H_b(x) = \begin{cases} J_c(x - \lambda_L) + H_e & \lambda_L < x < x_0 \\ J_{cr1}(x - x_0) & x_0 < x < x_1 \\ -J_{cm}(x - \lambda_L) + H_{em} & x_1 < x < d \end{cases}. \quad (34)$$

However, when $H_a > H_{fp}$, $H_b(x)$ is [Fig. 6(b)]

$$H_b(x) = J_c(x - \lambda_L) + H_e. \quad (35)$$

If $H_m > H_{fp}$ and $x_2 > d$, the remaining pinning current has only one direction. $H_s(x)$ is described by Eq. (32). When $H_a < H_{fp}$, $H_b(x)$ is [as shown in Fig. 6(c)]

$$H_b(x) = \begin{cases} J_c(x - \lambda_L) + H_e & \lambda_L < x < x_0 \\ J_{cr1}(x - x_0) & x_0 < x < d \end{cases}. \quad (36)$$

However, when $H_a > H_{fp}$, $H_b(x)$ is just as Eq. (35) [as shown in Fig. 6(c)].

Stage (vi). The field descending process in the negative side with H_a decreased from $-H_m$ to $-H_{c1}$. The superconductor is in mixed state and the field penetration process is the same as stage (iii), while both the magnetic field and the supercurrent have opposite direction.

Stage (vii). The vortex-trapped Meissner state with H_a firstly decreased from $-H_{c1}$ to 0 and then increased from 0 to H_{c1} . The remaining bulk pinning current density and the nonequilibrium magnetization are the same as stage (iv), while both the magnetic field and the supercurrent have opposite direction.

Stage (viii). The field ascending process in the positive side with H_a increased from H_{c1} to H_m . The superconductor is in mixed state and the field penetration process is the same as stage (v), while both the magnetic field and the supercurrent have opposite direction.

IV. CALCULATION OF TOTAL MAGNETIZATION

Based on the discussions mentioned above, the magnetization of superconducting plate can be calculated directly. Firstly, the total magnetization M is divided into two parts, i.e., the equilibrium magnetization M_{equ} and the nonequilibrium magnetization M_{pin} . For example, we take stage (ii) (the initial penetration process) into account, and other stages can be obtained in the same way. The field distribution of stage (ii) is shown in Fig. 7. We mark different parts of magnetization with different colored areas. The yellow area denotes the equilibrium magnetization M_{equ} , and the purple area denotes the nonequilibrium magnetization M_{pin} , respectively. In this case, we have M_{equ} and M_{pin} given by

$$M_{equ} = -\frac{1}{d}[H_a d - H_e(d - \lambda_L) - \int_0^{\lambda_L} H_s(x) dx], \quad (37)$$

$$M_{pin} = -\frac{1}{d}[H_e(d - \lambda_L) - \int_{\lambda_L}^d H_b(x) dx]. \quad (38)$$

Adding together these two different terms, we have the total magnetization M :

$$M = M_{equ} + M_{pin} = -\frac{1}{d}[H_a d - \int_0^{\lambda_L} H_s(x) dx - \int_{\lambda_L}^d H_b(x) dx]. \quad (39)$$

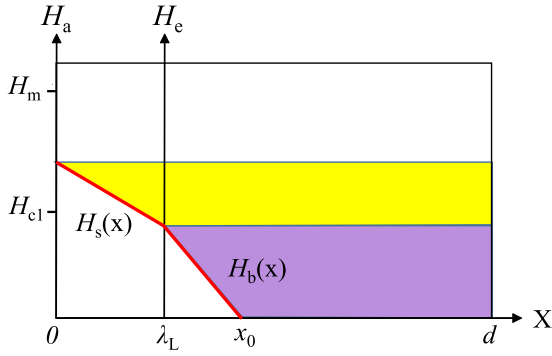


FIG. 7. Magnetic field distribution (red lines) of a superconductor in stage (ii) (the initial penetration process). The yellow area denotes the equilibrium magnetization M_{equ} , the purple area denotes the nonequilibrium magnetization M_{pin} , respectively.

With the field distribution $H_s(x)$ in the surface layer and $H_b(x)$ in the bulk region, the total magnetization can be calculated in this simple and effective way.

In this part, we will give the derivation of H_0 first appearing in Sec. II. According to our model, when H_a is reduced from a high value to below H_{c1} , the superconductor will try to re-enter the Meissner state. In this case, the magnetization will exhibit a linear dependence on H_a . But the slope of dM/dH_a is lower than that of the initial Meissner state. This is because the total magnetization of both the shielding part and the bulk pinning has a linear dependence on H_a . Actually, the characteristic field H_0 , which defines the field for remaining pinning current density reduces to zero in our model, can be obtained from the experimental data based on this logic. It is given by the field associating with the intersection point of linear parts from magnetization curves in the initial Meissner state and the vortex-trapped Meissner state [for example, stage (iv)] in the side of negative field. This can be understood in the following way. The total magnetization of the initial Meissner state is denoted as M_{ini} and given as

$$M_{\text{ini}} = -\frac{1}{d} \left[H_a d - \int_0^{\lambda_L} H_s(x) dx \right] = H_a \left(\frac{\lambda_L}{2d} - 1 \right). \quad (40)$$

The derivative of M_{ini} with H_a is constant $\lambda_L/2d - 1$. In this case, the linear relation of M_{ini} in the vicinity of $H_a = 0$ can be written as

$$M_{\text{ini},0} = H_a \frac{dM_{\text{ini}}}{dH_a} = H_a \left(\frac{\lambda_L}{2d} - 1 \right). \quad (41)$$

On the other hand, the magnetization of the vortex-trapped Meissner state [for example, Fig. 5(c) of stage (iv)] is denoted as M_{trp} . When $H_a < H_{c1}$, M_{trp} is given as

$$\begin{aligned} M_{\text{trp}} &= -\frac{1}{d} \left[H_a d - \int_0^{\lambda_L} H_s(x) dx - \int_{\lambda_L}^d H_b(x) dx \right] \\ &= H_a \left(\frac{\lambda_L}{2d} - 1 \right) + J_{c0} \frac{H_a - H_0}{H_{c1} - H_0} \frac{(d - \lambda_L)^2}{2d}. \end{aligned} \quad (42)$$

In the vicinity of $H_a = 0$, we have M_{trp}

$$M_{\text{trp}}|_{H_a=0} = J_{c0} \frac{-H_0}{H_{c1} - H_0} \frac{(d - \lambda_L)^2}{2d}. \quad (43)$$

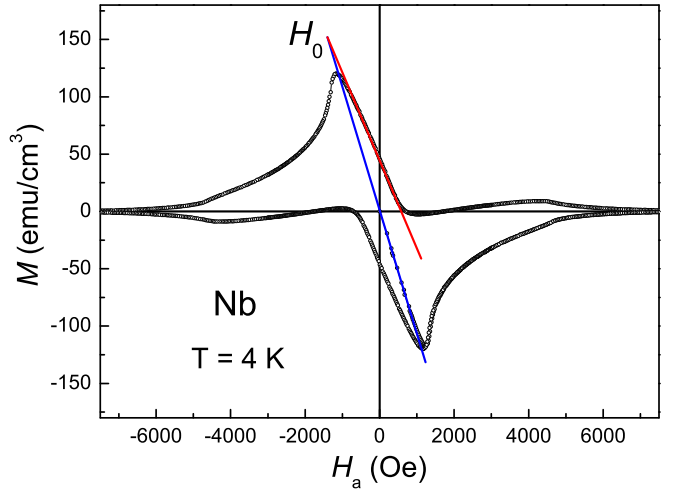


FIG. 8. An example showing how to determine the characteristic field H_0 , which is the field for the remaining bulk pinning current density J_{cr} to be zero. The black hollow points are the MHL of pure Nb at 4K from our experiments. The blue line is the linear relation of M_{ini} (magnetization of the initial Meissner state), the red line is the linear relation of M_{trp} (magnetization of the vortex-trapped Meissner state), and H_0 is the intersection point of the red line and blue line.

The derivative of M_{trp} at the field $H_a = 0$ is

$$\frac{dM_{\text{trp}}}{dH_a} \Big|_{H_a=0} = \left(\frac{\lambda_L}{2d} - 1 \right) + \frac{J_{c0}}{H_{c1} - H_0} \frac{(d - \lambda_L)^2}{2d}. \quad (44)$$

Thus the linear relation of M_{trp} in the vicinity of $H_a = 0$ can be written as

$$\begin{aligned} M_{\text{trp},0} &= H_a \frac{dM_{\text{trp}}}{dH_a} \Big|_{H_a=0} + M_{\text{trp}} \Big|_{H_a=0} \\ &= H_a \left[\left(\frac{\lambda_L}{2d} - 1 \right) + \frac{J_{c0}}{H_{c1} - H_0} \frac{(d - \lambda_L)^2}{2d} \right] \\ &\quad - \frac{J_{c0} H_0}{H_{c1} - H_0} \frac{(d - \lambda_L)^2}{2d}. \end{aligned} \quad (45)$$

It can be derived that, the intersection of these two straight lines [let $M_{\text{ini},0} = M_{\text{trp},0}$ from Eqs. (41) and (45)] gives rise to $H_a = H_0$. In this way, the value of H_0 is determined from experimental data, see an example in Fig. 8. It can be seen that, the characteristic field H_0 has a clear physical meaning and does not need to be treated as a fitting parameter.

In the end of this section, we will give some computed MHL curves of our model, as shown in Fig. 9. We changed the value of an individual parameter or ratio among H_m/H_{c1} , α , β , d/λ_L and demonstrated the corresponding change on the shape of MHL curves. For each case of change, we have shown results of two situations: $H_{c2}/H_{c1} = 5$ and $H_{c2}/H_{c1} = 1000$, as examples for low- κ and high- κ cases, respectively. For simplicity, all parameters are in unit of H_{c1} and d .

Figures 9(a) and 9(b) show two sets of MHLs at different values of H_m/H_{c1} . For both cases, $\alpha = 0.5$, $\beta = 0.5$, the zero-field critical current is $J_{c0} = 2H_{c1}/d$, and the thickness ratio is $d/\lambda_L = 1000$. The characteristic field is $H_0 = 2H_{c1}$ for $H_{c2}/H_{c1} = 5$ and $H_0 = 4H_{c1}$ for $H_{c2}/H_{c1} = 1000$. For $H_{c2}/H_{c1} = 5$ case shown in Fig. 9(a), five values of H_m/H_{c1}

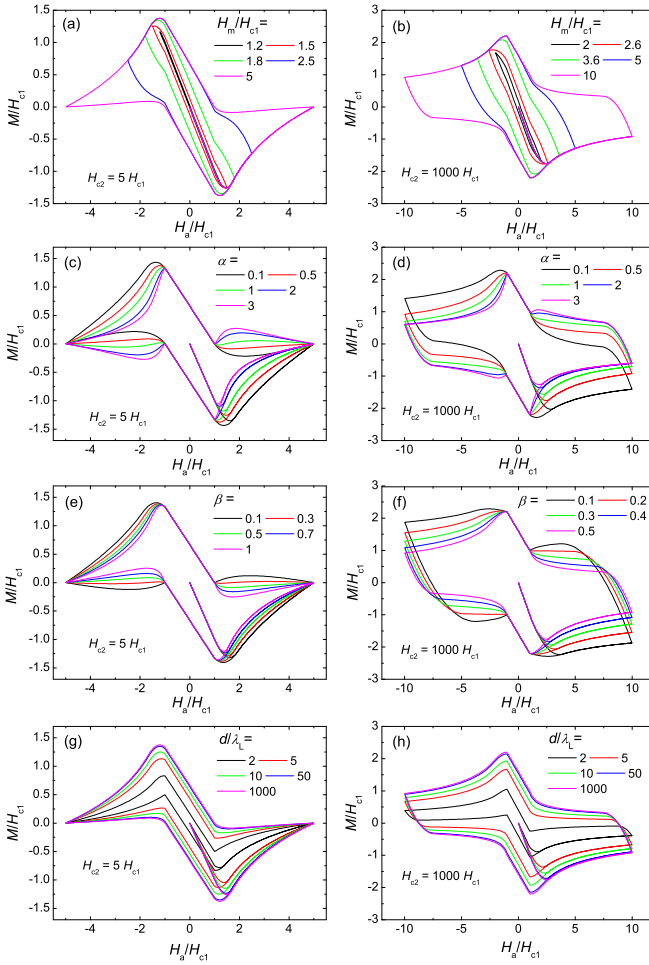


FIG. 9. Illustration of MHLs computed from our model: (a) H_m/H_{c1} dependence for $H_{c2}/H_{c1} = 5$, (b) H_m/H_{c1} dependence for $H_{c2}/H_{c1} = 1000$, (c) α dependence for $H_{c2}/H_{c1} = 5$, (d) α dependence for $H_{c2}/H_{c1} = 1000$, (e) β dependence for $H_{c2}/H_{c1} = 5$, (f) β dependence for $H_{c2}/H_{c1} = 1000$, (g) d/λ_L dependence for $H_{c2}/H_{c1} = 5$, and (h) d/λ_L dependence for $H_{c2}/H_{c1} = 1000$. Other fitting parameters are given in the text.

are chosen: 1.2, 1.5, 1.8, 2.5, 5. For $H_{c2}/H_{c1} = 1000$ case shown in Fig. 9(b), five values of H_m/H_{c1} are chosen: 2, 2.6, 3.6, 5, 10. It can be seen that, the MHLs are more like parallelogram when H_m is low and tend to be asymmetric with increasing H_m . In addition, the MHLs of $H_{c2}/H_{c1} = 5$ are more asymmetric than that of $H_{c2}/H_{c1} = 1000$.

Figures 9(c) and 9(d) show two sets of MHLs at different values of α . For both cases, β , J_{c0} , H_0 and d/λ_L are the same as Figs. 9(a) and 9(b), respectively. For $H_{c2}/H_{c1} = 5$ case shown in Fig. 9(c), $H_m = 5H_{c1}$ and five values of α are chosen: 0.1, 0.5, 1, 2, 3. For $H_{c2}/H_{c1} = 1000$ case shown in Fig. 9(d), $H_m = 10H_{c1}$ and five values of α are chosen: 0.1, 0.5, 1, 2, 3. The fitting parameter α is associated with the equilibrium magnetization. It can be seen that, with decreasing α , the asymmetry of MHLs is enhanced, while the width of MHLs along the H_a axis remains unchanged.

Figures 9(e) and 9(f) show two sets of MHLs at different values of β . For both cases, α , J_{c0} , H_0 and d/λ_L are the same as Figs. 9(a) and 9(b), respectively. For $H_{c2}/H_{c1} = 5$

case shown in Fig. 9(e), $H_m = 5H_{c1}$ and five values of β are chosen: 0.1, 0.3, 0.5, 0.7, 1. For $H_{c2}/H_{c1} = 1000$ case shown in Fig. 9(f), $H_m = 10H_{c1}$ and five values of α are chosen: 0.1, 0.2, 0.3, 0.4, 0.5. The fitting parameter β is associated with the nonequilibrium magnetization. It can be seen that, with decreasing β , the width of MHLs along the H_a axis for the vortex state is enlarged, while the asymmetry of MHLs remains unchanged.

Figures 9(g) and 9(h) show two sets of MHLs at different values of d/λ_L . For both cases, α , β , J_{c0} and H_0 are the same as Figs. 9(a) and 9(b), respectively. For $H_{c2}/H_{c1} = 5$ case shown in Fig. 9(g), $H_m = 5H_{c1}$ and five values of d/λ_L are chosen: 2, 5, 10, 50, 1000. For $H_{c2}/H_{c1} = 1000$ case shown in Fig. 9(h), $H_m = 10H_{c1}$ and five values of d/λ_L are chosen: 2, 5, 10, 50, 1000. d is half thickness of sample. And it can be seen that, with decreasing thickness of sample, the initial Meissner curve tends to deviate from the linear line more earlier before H_a achieves H_{c1} , and the MHL tends to be thinner. The latter indicates that, both the nonequilibrium magnetization and the flux pinning are significantly reduced with decreasing thickness of sample. When d/λ_L is beyond 50, the MHL remains almost unchanged and this indicates that the effect of thickness is vanished. On the other hand, when the thickness is decreased to the same scale of London penetration depth, the critical field of the superconductor will change at the same time [48], which is not considered in our model.

To summarize for this section, we can simulate the flux penetrating process and fit the MHLs of type-II superconductors well by using proper fitting parameters. This plays an important role in studying the physical properties of type-II superconductors.

V. EXPERIMENTS AND MODEL FITS

In the fitting to a global MHL at a fixed temperature, there are generally six fitting parameters: α , β , H_{c1} , H_{c2} , J_{c0} , and H_0 . Each quantity can be obtained through a fitting to a specific property or MHL curve in a certain period. Firstly, H_{c1} can be roughly determined from the field where the initial $M(H)$ curve starts to deviate from the linear Meissner line. H_0 can also be obtained from the intersecting point of the initial Meissner line and the vortex-trapped Meissner line (in the field descending process) based on our model (refers to Secs. II and IV). In principle, the upper critical field H_{c2} can be determined from the field where the magnetization vanishes to zero. This is easy for superconductors with small values of H_{c2} , such as Nb. However, if H_{c2} is very large and cannot be directly determined from the experiment data, we have to adopt a value of H_{c2} from the published literatures (mainly from the high field transport measurements).

Secondly, the two branches of MHL in the regions with positive fields, including field ascending magnetization M_{up} and field descending magnetization M_{down} , are added up to derive the equilibrium magnetization $M_{equ} = (M_{up} + M_{down})/2$ [13,29]. This is because the nonequilibrium magnetization in these two branches due to bulk pinning have roughly the same value but opposite signs based on Bean critical state model, and we can use this simple relation to calculate the equilibrium magnetization M_{equ} . Once M_{equ} is obtained,

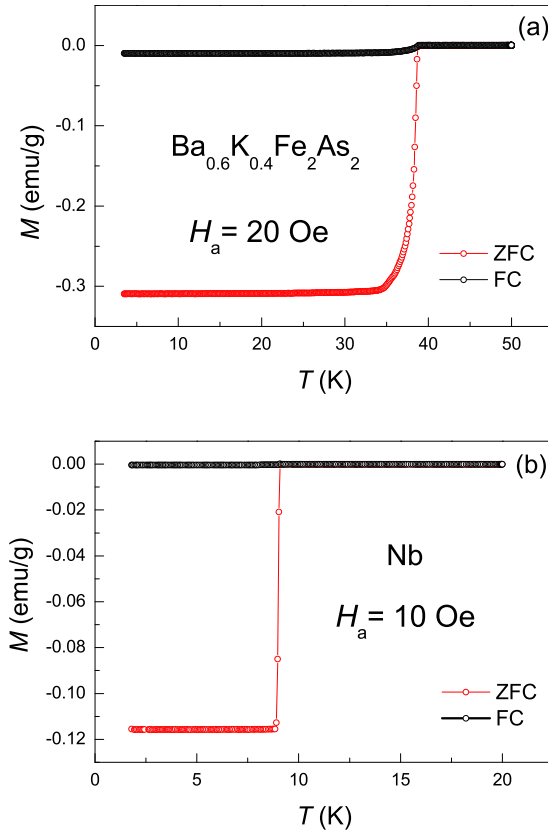


FIG. 10. Temperature dependence of magnetization measured with zero-field cooled (ZFC) and field cooled (FC) modes for (a) the $\text{Ba}_{0.6}\text{K}_{0.4}\text{Fe}_2\text{As}_2$ single crystal and (b) the pure Nb plate. The applied field is parallel to the biggest plane of sample.

we can fit M_{equ} with Eq. (1) and obtain the fitting parameter α , together with a slight modification to the already obtained H_{c1} , especially in the low-field region.

Thirdly, the nonequilibrium magnetization of the field ascending process in the positive side can also be obtained by $M_{\text{pin}} = M_{\text{up}} - M_{\text{equ}}$ or $M_{\text{pin}} = (M_{\text{up}} - M_{\text{down}})/2$. When the sample is fully penetrated by magnetic vortices ($H_a > H_{\text{fp}}$), the nonequilibrium magnetization M_{pin} in our model is

$$\begin{aligned} M_{\text{pin}} &= \frac{J_c(d - \lambda_L)^2}{2d} \\ &= \frac{J_{c0}(d - \lambda_L)^2 H_{c2} - |H_e|}{2d H_{c2}} \left(\frac{H_{c1}}{H_{c1} + |H_e|} \right)^\beta \\ &= M_{\text{pin}0} \frac{H_{c2} - |H_e|}{H_{c2}} \left(\frac{H_{c1}}{H_{c1} + |H_e|} \right)^\beta. \end{aligned} \quad (46)$$

We have used Eq. (10) and $M_{\text{pin}0} = J_{c0}(d - \lambda_L)^2/(2d)$. In this way, we can use Eq. (46) to fit the M_{equ} obtained from experiment data and determine the fitting parameters β and J_{c0} . There should be a conversion from H_a to H_e by Eqs. (1) and (2) in the fitting to M_{pin} . On the other hand, J_{c0} is associated with the remaining bulk pinning current J_{cr} at $H_a = 0$ by Eq. (12). The J_{cr} at $H_a = 0$ can be roughly calculated from the Bean critical state model. Finally, with all six parameters obtained, we can fit the global MHL curve. In the final process, we should slightly adjust all fitting parameters to get a global

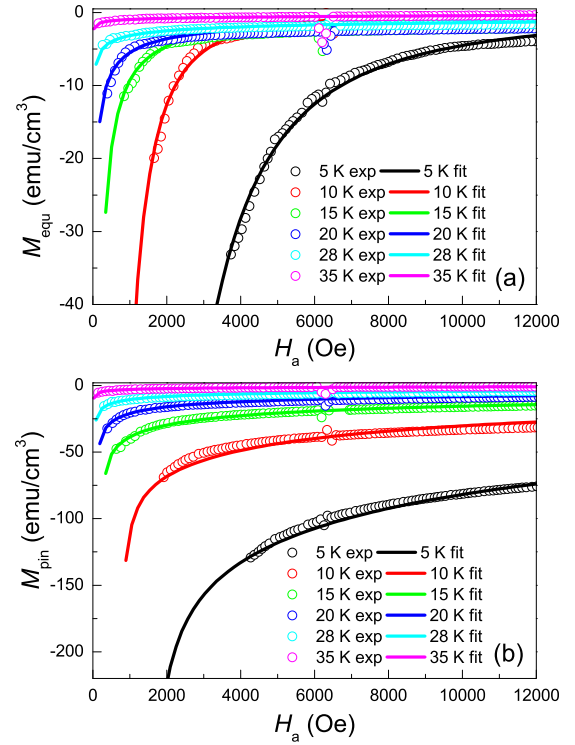


FIG. 11. (a) Fitting to the equilibrium magnetization of the $\text{Ba}_{0.6}\text{K}_{0.4}\text{Fe}_2\text{As}_2$ single crystal in the vortex state at different temperatures: experiment data (hallow points) and fitting curves (lines). (b) Fitting to the nonequilibrium magnetization of the $\text{Ba}_{0.6}\text{K}_{0.4}\text{Fe}_2\text{As}_2$ single crystal in the field ascending process at different temperatures: experiment data (hallow points) and fitting curves (lines).

fitting to the MHL curve in all periods and this adjustment should be fed back to each fitting process mentioned above simultaneously, in order to minimize the influence of this adjustment. Above all, the MHLs of a superconductor can be fitted by our model.

To check how effective of our model is, MHLs of two kinds of superconductors are studied. We chose a pure Nb plate as a test sample for the low- κ case and a $\text{Ba}_{0.6}\text{K}_{0.4}\text{Fe}_2\text{As}_2$ single crystal ($\kappa_{\text{ab}} = 260$ [49]) as a test sample for extremely high- κ case. The $\text{Ba}_{0.6}\text{K}_{0.4}\text{Fe}_2\text{As}_2$ single crystal was grown by self-flux method using FeAs as flux [50], with dimensions $1.8 \text{ mm} \times 1.1 \text{ mm} \times 0.15 \text{ mm}$ and weight 1.7 mg . The pure Nb plate was prepared by arc-melting method and then cut into rectangular shape by wire cutting machine, with dimensions $3.5 \text{ mm} \times 2.9 \text{ mm} \times 0.42 \text{ mm}$ and weight 40.7 mg . The DC magnetization measurements were carried out on a SQUID-VSM-7T (Quantum Design). The applied field was parallel to the biggest plane of samples. The temperature dependence of magnetization $M(T)$ for both samples are shown in Fig. 10, respectively. The sharp transition indicates that both samples are of high quality. The obtained critical temperature T_c for the $\text{Ba}_{0.6}\text{K}_{0.4}\text{Fe}_2\text{As}_2$ is 38.5 K which indicates that the sample is close to the optimal doping point [50], and for Nb is 9 K . We need to note that, a small tail on the transition curve of the $\text{Ba}_{0.6}\text{K}_{0.4}\text{Fe}_2\text{As}_2$ makes the transition a little broad, but we find that this feature is intrinsic, since

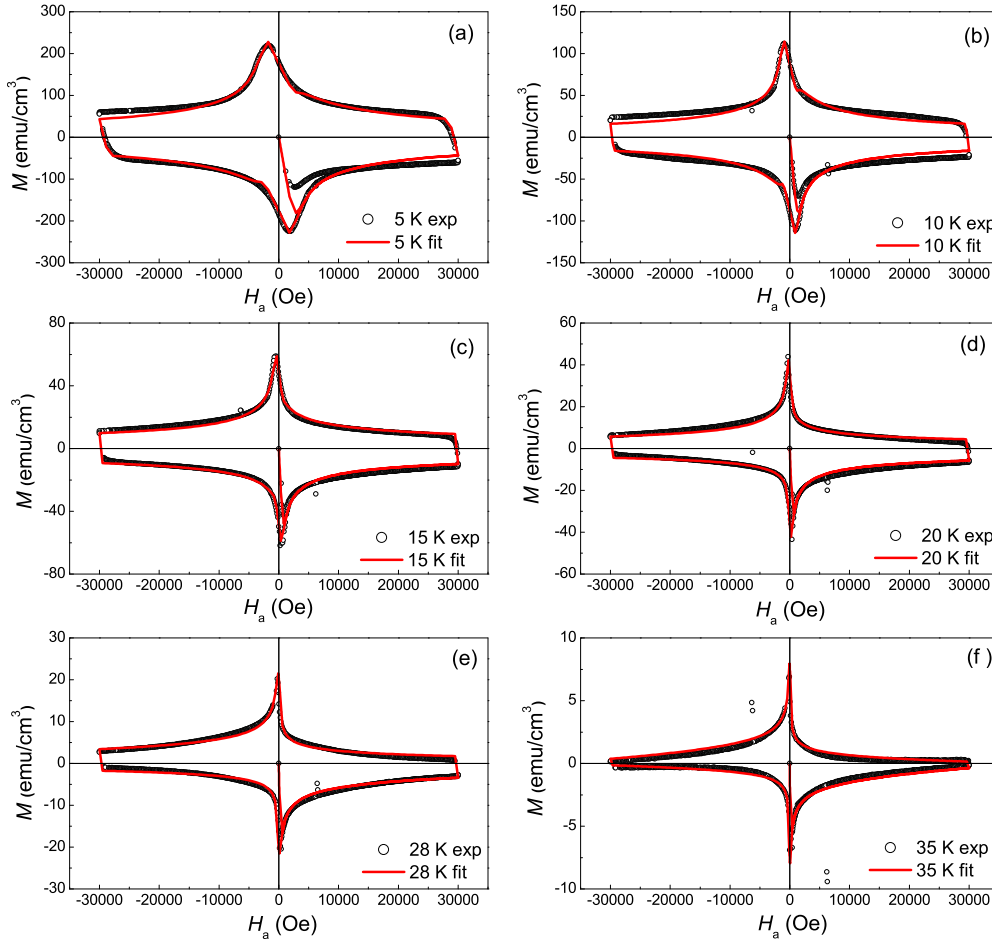


FIG. 12. The MHLs (black hallow points) and corresponding fitting curves (red lines) of the $\text{Ba}_{0.6}\text{K}_{0.4}\text{Fe}_2\text{As}_2$ single crystal, at temperatures of (a) 5, (b) 10, (c) 15, (d) 20, (e) 28, and (f) 35 K. A small background magnetization due to the induced magnetic field of the measuring coils has been subtracted for all temperatures, which was measured with no sample on the sample holder.

the transition curve when the field is perpendicular to the biggest plane looks very sharp. This tail may be attributed to a divergent London penetration depth when temperature approaches T_c .

Figures 11(a) and 11(b) shows fittings to the equilibrium magnetization and the nonequilibrium magnetization of the $\text{Ba}_{0.6}\text{K}_{0.4}\text{Fe}_2\text{As}_2$ single crystal in the low-field region and intermediate-field region, respectively. Figure 12 shows the global fitting to MHLs of the $\text{Ba}_{0.6}\text{K}_{0.4}\text{Fe}_2\text{As}_2$ single crystal, including six different temperatures: 5, 10, 15, 20, 28, and 35K. A small background magnetization due to the induced magnetic field of the measuring coils has been subtracted from the raw data of MHLs for all temperatures, which was measured with no sample on the sample holder. All six fitting parameters used in the fitting process are shown in Table I, including the lower critical field H_{c1} , the upper critical field H_{c2} , the characteristic field H_0 , the zero-field critical current density J_{c0} , the exponents α and β . The London penetration depth used in the fitting process is $\lambda_L = 300$ nm which is determined from MFM measurements of the similar sample [51]. We assume the London penetration depth to be independent of temperature for simplicity. This is a good approximation as the London penetration depth λ_L is much smaller than the

thickness of our sample $2d$ ($2d = 0.15$ mm, $\lambda_L \ll 2d$). It can be seen in Figs. 11 and 12 that the fitting curves accord well with the equilibrium magnetization and the nonequilibrium magnetization, as well as the global MHLs for almost all temperatures. In addition, we find that the MHL curves become more asymmetric when the measuring temperature is higher. This indicates that, the ratio of equilibrium magnetization in the total magnetization rises with increasing temperature [30,36,37]. On the other hand, the nonequilibrium magnetization plays the leading role at temperatures lower than 10K,

TABLE I. The fitting parameters of the $\text{Ba}_{0.6}\text{K}_{0.4}\text{Fe}_2\text{As}_2$ single crystal.

T (K)	H_{c1} (Oe)	$H_{c2}(T)$	H_0 (Oe)	J_{c0} (A/cm ²)	α	β
5	1780	80	3490	7.17×10^5	1.99	0.62
10	890	71	1780	3.53×10^5	2.13	0.58
15	344	55	970	1.78×10^5	1.01	0.42
20	188	43	810	1.18×10^5	0.60	0.41
28	89	16	314	6.95×10^4	0.33	0.36
35	28	4	112	2.57×10^4	0.23	0.32

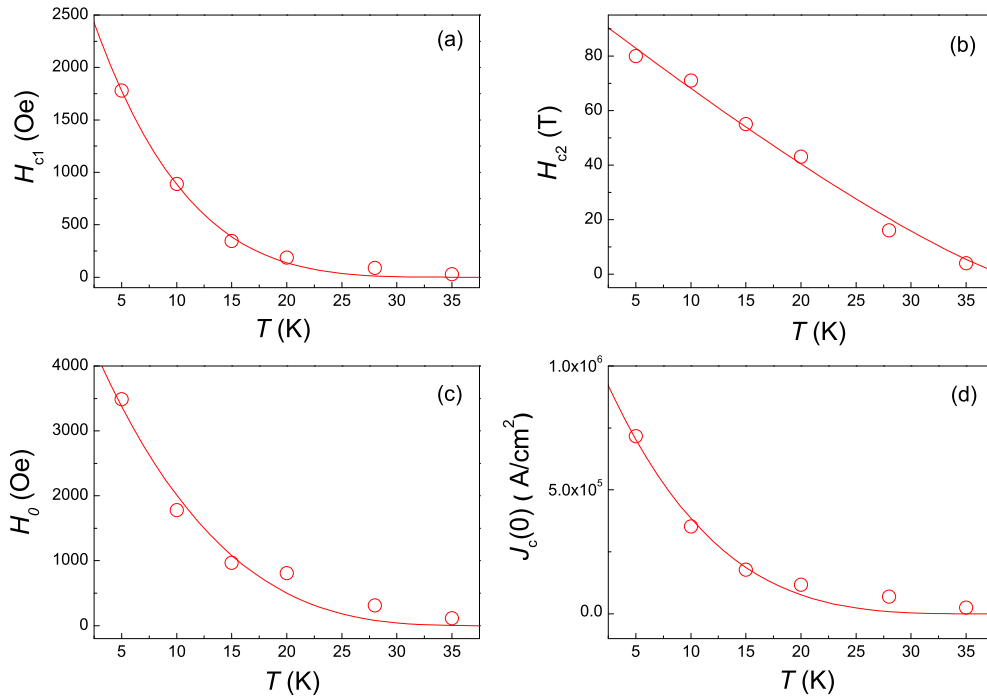


FIG. 13. Temperature dependence of different fitting parameters for the Ba_{0.6}K_{0.4}Fe₂As₂ single crystal. (a) H_{c1} , (b) H_{c2} , (c) H_0 , and (d) J_{c0} . The red circles are fitting parameters at different temperatures. The red lines are empirical scaling relations.

which leads to the symmetric shape of MHLs with respect to the H_a axis [12,13]. The fitting parameters α and β govern the decaying rate of the magnetization versus external field in the equilibrium and nonequilibrium process. Due to their different mechanisms, their values and behaviors with temperature should be very different. Taking the equilibrium magnetization in the low field region into account, the parameter α can be quite large as its rapid decaying rate at a low temperature. But when temperature increases, the equilibrium magnetization curve $M_{\text{equ}}(H)$ becomes flat quickly, and thus α reduces significantly, which is shown in Fig. 11(a) and Table I. As a comparison, the parameter β is related to the flux pinning of superconductors and determined by fitting to the nonequilibrium magnetization $M_{\text{pin}}(H)$ in the intermediate and high field region. It can be seen in Fig. 11(b) that the nonequilibrium magnetization $M_{\text{pin}}(H)$ decays slowly with increasing field both at low temperature and high temperature. In this case, the change of parameter β is relatively small.

Figure 13 shows the temperature dependence of H_{c1} , H_{c2} , H_0 , J_{c0} for the Ba_{0.6}K_{0.4}Fe₂As₂ single crystal and the corresponding fitting curves based on the empirical scaling relation $H(T) = H(0)(1 - T/T_c)^n$. In this case, we obtained the following fitting parameters: $H_{c1}(0) = 3235$ Oe and $n = 4.31$ for $H_{c1}(T)$, $H_{c2}(0) = 98$ T and $n = 1.21$ for $H_{c2}(T)$, $H_0(0) = 5276$ Oe and $n = 3.21$ for $H_0(T)$, $J_{c0}(0) = 1.19 \times 10^6$ A/cm² and $n = 3.73$ for $J_{c0}(T)$, respectively. The obtained value of $H_{c1}(0)$ is much higher than that given by Ren [52] of similar superconductor (with $T_c = 36.2$ K, lower than 38.5 K of our sample). The value of $H_{c2}(0)$ is lower than that predicted by Wang (235 T) [53] and Ishida (300 T) [9], but higher than that given by Altarawneh *et al.* (75 T) [54]. Unfortunately, there are no direct measurements about the H_{c2} of Ba_{0.6}K_{0.4}Fe₂As₂

at low temperatures since it is really too high. In the fitting process of Ba_{0.6}K_{0.4}Fe₂As₂, we use the value of H_{c2} from the published literatures [55,56] at the beginning; we gradually reduce the value of H_{c2} until the fitting curves start to deviate from the experiment data obviously. In this way, the H_{c2} used in the fitting can serve as a reference to the lowest limit of the upper critical field for achieving a good fit. The zero-field critical current density at 0K is $J_{c0}(0) = 1.19 \times 10^6$ A/cm², which is close to those given by others [9,17] obtained directly through the original Bean critical state model.

Figures 14(a) and 14(b) shows fittings to the equilibrium magnetization and the nonequilibrium magnetization of the pure Nb plate, respectively. Figure 15 shows the global fitting to MHLs of the pure Nb plate, including two temperatures: 4 and 6 K. A small background magnetization arising from the sample holder has also been subtracted from the raw data of MHLs for all temperatures. All six fitting parameters of Nb are shown in Table II. The London penetration depth used in the fitting process is $\lambda_L = 40$ nm from published literatures [57] and we have $\lambda_L \ll 2d$ ($2d = 0.42$ mm). However, it can be seen in Fig. 14 that, the field where the equilibrium magnetization vanishes to zero is not equal to the field where the nonequilibrium magnetization vanishes to zero, the former is 5100 Oe and the latter is 8500 Oe for 4 K and 3000 Oe and

TABLE II. The fitting parameters of the pure Nb plate.

T (K)	H_{c1} (Oe)	H_{c2} (Oe)	H_0 (Oe)	J_{c0} (A/cm ²)	α	β
4	910	6800	1400	5.91×10^4	1.35	0.67
6	580	4400	800	3.57×10^4	1.16	0.77

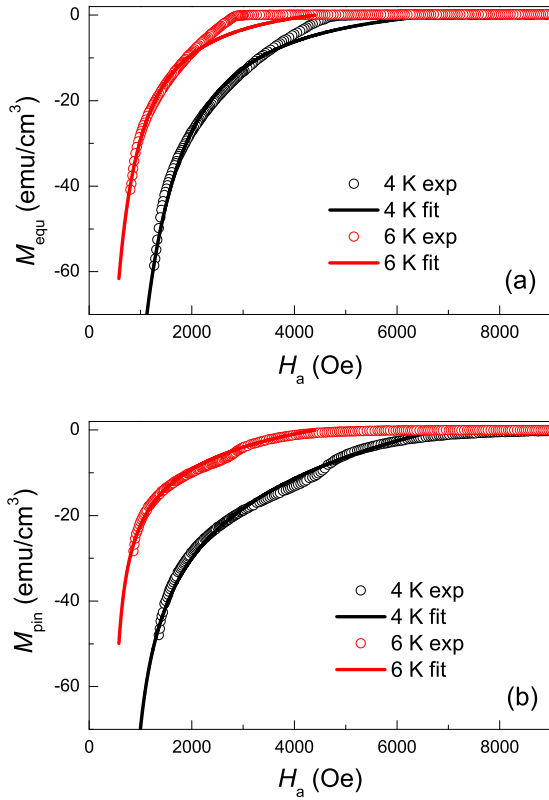


FIG. 14. (a) Fitting to the equilibrium magnetization of the pure Nb plate in the vortex state at different temperatures: experiment data (hallow points) and fitting curves (lines). (b) Fitting to the nonequilibrium magnetization of the pure Nb plate in the field ascending period at different temperatures: experiment data (hallow points) and fitting curves (lines).

5800 Oe for 6 K, respectively. This may be attributed to the possible enhancement of vortex pinning due to second peak effect near H_{c2} in Nb [58–60]. This can be corroborated from the data of the nonequilibrium magnetization data shown in Fig. 14(b). For simplicity, we take the average value of these two fields as H_{c2} for each temperature. It can be seen that, the fitting curves in Figs. 14 and 15 all accord well with the experiment data. The value of H_{c1} in Table II is a little lower than that of high-purity Nb, while the value of H_{c2} is slightly higher than that in previous reports [29,61]. In addition, the fitting parameter α decreases slightly with increasing temperature, while the fitting parameter β increases slightly.

From above analysis and fitting to the experimental data, we find that our model which counts different magnetization from the surface layer and the bulk pinning region is quite effective. Although the model is quite simple in form, it can capture the fundamental physics of both regions with different contributions of magnetization. By adjusting fitting parameters and proportion of two parts of magnetization, our model can be used to describe the flux penetration and magnetization of various type-II superconductors with different values of κ or ratios of H_{c2}/H_{c1} . For further verification of our model, more experiments on different superconductors are highly desired. In addition, the difference between simulated curve and experimental data near H_{c1} in low temperature region

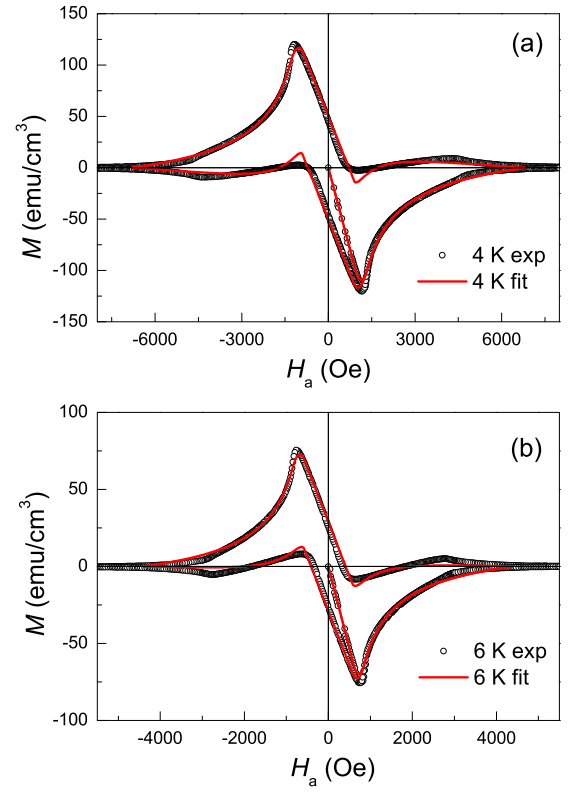


FIG. 15. MHLs (black hallow points) and corresponding fitting curves (red lines) of the pure Nb plate, at temperatures of (a) 4 and (b) 6 K. A small background magnetization due to the induced magnetic field of the measuring coils has been subtracted for all temperatures, which was measured with no sample on the sample holder.

may involve the influence of the Bean-Livingston surface barrier [62] or geometrical barrier [63,64], on which further experiments are needed. The enhancement of magnetization due to these effects occurs mainly in the flux entry process, as shown by our experimental data, but unfortunately it cannot be explicitly expressed so far. This Bean-Livingston related effect in the AC losses of type-II superconductors were dealt by Clem [65]. In the case of DC magnetization measurements and with a strong bulk pinning, this effect is weak comparing with the large magnetization due to the bulk pinning and occurs only in the initial penetration process, thus it will merge into the effective first penetration magnetic field, and H_{c1} may be modified by adding an extra term, namely $H_{\text{Bean-Livingston}} = H_{c1} + \Delta H$. This little deviation may be just reflected by the small discrepancy in low field region, as shown in Fig. 15. Our present model can describe the global MHLs pretty well and may be extended to other type-II superconductors when a global description on MHLs is needed.

VI. CONCLUSION

In summary, a generalized phenomenological model for critical vortex state has been proposed to describe the magnetic field penetration and MHLs of type-II superconductors. The model combines the equilibrium magnetization of surface screening current and the nonequilibrium magnetization of

bulk pinning, and deals with the vortex-trapped Meissner state in a more reasonable way. We use the model to simulate the MHLs of extremely high- κ superconductor $\text{Ba}_{0.6}\text{K}_{0.4}\text{Fe}_2\text{As}_2$ and low- κ superconductor Nb and the experimental data can both be fitted quite well. Furthermore, our model can serve as an effective tool to study the magnetization hysteresis and vortex penetration of type-II superconductors with different values of κ or ratios of H_{c2}/H_{c1} .

ACKNOWLEDGMENTS

We appreciate the fruitful discussions with Alex Gurevich and Vitalii Vlasko-Vlasov. This work was supported by the National Natural Science Foundation of China (Grants No. A0402/11927809, No. A0402/11534005), National Key R and D Program of China (Grant No. 2016YFA0300401), and the Strategic Priority Research Program of Chinese Academy of Sciences (Grant No. XDB25000000).

-
- [1] A. A. Abrikosov, *J. Exp. Theor. Phys. U. S. S. R.* **32**, 1442 (1957).
- [2] V. L. Ginzburg and L. D. Landau, *Zh. Eksp. Teor. Fiz.* **20**, 1064 (1950).
- [3] A. P. Banford and G. H. Stafford, *J. Nucl. Energy. C* **3**, 287 (1961).
- [4] D. B. Liarte, S. Posen, M. K. Transtrum *et al.*, *Supercond. Sci. Technol.* **30**, 033002 (2017).
- [5] G. Blatter, M. V. Feigel'man, V. B. Geshkenbein, A. I. Larkin, and V. M. Vinokur, *Rev. Mod. Phys.* **66**, 1125 (1994).
- [6] R. Griessen, W. Hai-hu, A. J. J. Van Dalen, B. Dam, J. Rector, and H. G. Schnack, S. Libbrecht, E. Osquiguil, and Y. Bruynseraede, *Phys. Rev. Lett.* **72**, 1910 (1994).
- [7] H. H. Wen, X. S. Rong, B. Yin, G. C. Che, and Z. X. Zhao, *Physica C* **242**, 365 (1995).
- [8] L. Fang, Y. Jia, C. Chaparro, G. Sheet, H. Claus, M. A. Kirk, A. E. Koshelev, U. Welp, G. W. Crabtree, W. K. Kwok, S. Zhu, H. F. Hu, J. M. Zuo, H. H. Wen, and B. Shen, *Appl. Phys. Lett.* **101**, 012601 (2012).
- [9] S. Ishida, D. Song, H. Ogino, A. Iyo, H. Eisaki, M. Nakajima, J.-i. Shimoyama, and M. Eisterer, *Phys. Rev. B* **95**, 014517 (2017).
- [10] A. Takahashi, S. Pyon, T. Kambara, A. Yoshida, and T. Tamegai, *J. Phys. Soc. Jpn.* **89**, 094705 (2020).
- [11] H. Huang, C. Yao *et al.*, *Supercond. Sci. Technol.* **31**, 015017 (2018).
- [12] C. P. Bean, *Phys. Rev. Lett.* **8**, 250 (1962).
- [13] C. P. Bean, *Rev. Mod. Phys.* **36**, 31 (1964).
- [14] H. London, *Phys. Lett.* **6**, 162 (1963).
- [15] J. E. Evetts, A. M. Campbell, and D. Dew-Hughes, *Phil. Mag.* **10**, 339 (1964).
- [16] H. H. Wen and Z. X. Zhao, *Appl. Phys. Lett.* **68**, 856 (1996).
- [17] W. Cheng, H. Lin, B. Shen, and H. H. Wen, *Sci. Bull.* **64**, 81 (2019).
- [18] Y. B. Kim, C. F. Hempstead, and A. R. Strnad, *Phys. Rev. Lett.* **9**, 306 (1962).
- [19] Y. B. Kim, C. F. Hempstead, and A. R. Strnad, *Phys. Rev.* **129**, 528 (1963).
- [20] P. W. Anderson, *Phys. Rev. Lett.* **9**, 309 (1962).
- [21] P. W. Anderson and Y. B. Kim, *Rev. Mod. Phys.* **36**, 39 (1964).
- [22] J. H. P. Watson, *J. Appl. Phys.* **39**, 3406 (1968).
- [23] F. Irie and K. Yamafuji, *J. Phys. Soc. Jpn.* **23**, 255 (1976).
- [24] I. M. Green and P. Hlwaiczka, *Proc. IEE* **144**, 1329 (1967).
- [25] W. A. Fietz, M. R. Beasley, J. Silcox, and W. W. Webb, *Phys. Rev.* **136**, A335 (1964).
- [26] V. R. Karasik, N. G. Vasil'ev, and V. G. Ershov, *Zh. Eksp. Teor. Fiz.* **59**, 790 (1970).
- [27] D. X. Chen, A. Sanchez, and J. S. Munoz, *J. Appl. Phys.* **67**, 3430 (1990).
- [28] M. Xu, D. L. Shi, and R. F. Fox, *Phys. Rev. B* **42**, 10773(R) (1990).
- [29] P. H. Kes, C. A. M. van der Klein, and D. de Klerk, *J. Low. Tem. Phys.* **10**, 759 (1973).
- [30] D. X. Chen, R. W. Cross, and A. Sanchez, *Cryogenics* **33**, 695 (1993).
- [31] D. X. Chen, R. B. Goldfarb, R. W. Cross, and A. Sanchez, *Phys. Rev. B* **48**, 6426 (1993).
- [32] M. Sinder, V. Meerovich, V. Sokolovsky, and I. Vajda, *IEEE Trans. Appl. Supercond.* **9**, 4661 (1999).
- [33] V. M. Krasnov and V. V. Ryazanov, *Physica C* **297**, 153 (1998).
- [34] Y. Kimishima and Y. Ichianagi, *Physica C* **353**, 111 (2001).
- [35] Y. Kimishima, H. Ichikawa, S. Takano, and T. Kuramoto, *Supercond. Sci. Technol.* **17**, S36 (2004).
- [36] D. M. Gokhfeld, D. A. Balaev, M. I. Petrov, S. I. Popkov, K. A. Shaykhutdinov, and V. V. Val'kov, *J. Appl. Phys.* **109**, 033904 (2011).
- [37] D. M. Gokhfeld, *Phys. Solid. State.* **56**, 2380 (2014).
- [38] T. Matsushita and K. Yamafuji, *J. Phys. Soc. Jpn.* **46**, 764 (1979).
- [39] G. P. Mikitik and E. H. Brandt, *Phys. Rev. B* **62**, 6812 (2000).
- [40] D. X. Chen, A. Hernando, F. Conde, J. Ramirez, J. M. Gonzalez-Calbet, and M. Vallet, *J. Appl. Phys.* **75**, 2578 (1994).
- [41] F. London and H. London, *Proc. Roy. Soc.* **A155**, 71 (1935).
- [42] Z. D. Hao, J. R. Clem, M. W. McElfresh, L. Civale, A. P. Malozemoff, and F. Holtzberg, *Phys. Rev. B* **43**, 2844 (1991).
- [43] Z. D. Hao and J. R. Clem, *Phys. Rev. Lett.* **67**, 2371 (1991).
- [44] A. M. Campbell, J. E. Evetts, and D. Dew-Hughes, *Phil. Mag.* **10**, 333 (1964).
- [45] J. D. Livingston, *Phys. Rev.* **129**, 1943 (1963).
- [46] D. G. Walmsley, *J. appl. Phys.* **43**, 615 (1972).
- [47] R. Prozorov and V. G. Kogan, *Phys. Rev. Appl.* **10**, 014030 (2018).
- [48] G. Stejic, A. Gurevich, E. Kadyrov, D. Christen, R. Joynt, and D. C. Larbalestier, *Phys. Rev. B* **49**, 1274 (1994).
- [49] U. Welp, R. Xie, A. E. Koshelev, W. K. Kwok, H. Q. Luo, Z. S. Wang, G. Mu, and H. H. Wen, *Phys. Rev. B* **79**, 094505 (2009).
- [50] H. Q. Luo, Z. S. Wang, H. Yang, P. Cheng, X. Y. Zhu, and H. H. Wen, *Supercond. Sci. Technol.* **21**, 125014 (2008).
- [51] A. Almoalem, A. Yagil, K. Cho, S. Teknowijoyo, M. A. Tanatar, R. Prozorov, Y. Liu, T. A. Lograsso, and O. M. Auslaender, *Phys. Rev. B* **98**, 054516 (2018).
- [52] C. Ren, Z. S. Wang, H. Q. Luo, H. Yang, L. Shan, and H. H. Wen, *Physica C* **469**, 599 (2009).
- [53] Z. S. Wang, H. Q. Luo, C. Ren, and H. H. Wen, *Phys. Rev. B* **78**, 140501(R) (2008).

- [54] M. M. Altarawneh, K. Collar, C. H. Mielke, N. Ni, S. L. Bud'ko, and P. C. Canfield, *Phys. Rev. B* **78**, 220505(R) (2008).
- [55] A. Gurevich, *Nat. Mater.* **10**, 255 (2011).
- [56] C. Tarantini, A. Gurevich, J. Jaroszynski, F. Balakirev, E. Bellingeri, I. Pallecchi, C. Ferdeghini, B. Shen, H. H. Wen, and D. C. Larbalestier, *Phys. Rev. B* **84**, 184522 (2011).
- [57] A. Valente-Felicianom, *Supercond. Sci. Technol.* **29**, 113002 (2016).
- [58] W. DeSorbo, *Phys. Rev.* **132**, 107 (1963).
- [59] W. DeSorbo, *Rev. Mod. Phys.* **36**, 90 (1964).
- [60] P. L. Gammel, U. Yaron, A. M. Chang *et al.*, *Phys. Rev. Lett.* **80**, 833 (1998).
- [61] D. K. Finnemore, T. F. Stromberg, and C. A. Swenson, *Phys. Rev.* **149**, 231 (1966).
- [62] C. P. Bean and J. D. Livingston, *Phys. Rev. Lett.* **12**, 14 (1964).
- [63] D. Majer, E. Zeldov, M. Konczykowski *et al.*, *Physica C* **235**, 2765 (1994).
- [64] E. Zeldov, A. I. Larkin, V. B. Geshkenbein, M. Konczykowski, D. Majer, B. Khaykovich, V. M. Vinokur, and H. Shtrikman, *Phys. Rev. Lett.* **73**, 1428 (1994).
- [65] J. R. Clem, *J. Appl. Phys.* **50**, 3518 (1979).